

Binding branched and linear DNA structures: From isolated clusters to fully bonded gels

J. Fernandez-Castanon, F. Bomboi, and F. Sciortino

Citation: *The Journal of Chemical Physics* **148**, 025103 (2018);

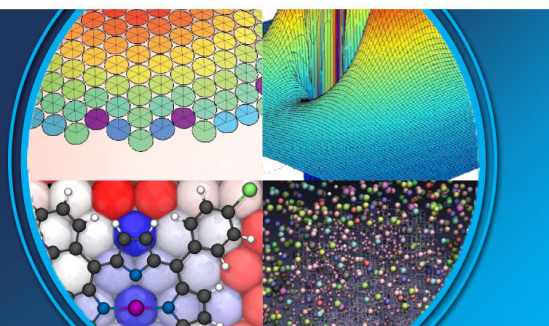
View online: <https://doi.org/10.1063/1.5011720>

View Table of Contents: <http://aip.scitation.org/toc/jcp/148/2>

Published by the [American Institute of Physics](#)

AIP | The Journal of
Chemical Physics

PERSPECTIVES



Binding branched and linear DNA structures: From isolated clusters to fully bonded gels

J. Fernandez-Castanon,^{1,a)} F. Bomboi,¹ and F. Sciortino^{1,2}

¹Physics Department, Sapienza–Università di Roma, Piazzale Aldo Moro 5, 00185 Rome, Italy

²CNR-ISC, UOS Sapienza–Università di Roma, 00186 Rome, Italy

(Received 2 November 2017; accepted 11 December 2017; published online 9 January 2018)

The proper design of DNA sequences allows for the formation of well-defined supramolecular units with controlled interactions via a consecution of self-assembling processes. Here, we benefit from the controlled DNA self-assembly to experimentally realize particles with well-defined valence, namely, tetravalent *nanostars* (*A*) and bivalent *chains* (*B*). We specifically focus on the case in which *A* particles can only bind to *B* particles, via appropriately designed sticky-end sequences. Hence *AA* and *BB* bonds are not allowed. Such a binary mixture system reproduces with DNA-based particles the physics of poly-functional condensation, with an exquisite control over the bonding process, tuned by the ratio, *r*, between *B* and *A* units and by the temperature, *T*. We report dynamic light scattering experiments in a window of *T*s ranging from 10 °C to 55 °C and an interval of *r* around the percolation transition to quantify the decay of the density correlation for the different cases. At low *T*, when all possible bonds are formed, the system behaves as a fully bonded network, as a percolating gel, and as a cluster fluid depending on the selected *r*. *Published by AIP Publishing.* <https://doi.org/10.1063/1.5011720>

I. INTRODUCTION

Starting from the seminal work of Seeman,¹ several complex all DNA-made nanoparticles have been designed and realized in the laboratories. These novel colloidal particles have potential applications in several fields due to their ability to operate at the nanoscale.^{2,3} The possibility to selectively control the binding of complementary sequences and the different pairing ability of strands with different number of nucleotides are key elements in DNA design.

Besides technological applications, DNA-made particles can be tailored to convert *in charta* or *in silico* intuitions into experimental realizations.^{4,5} Indeed, it is not only possible to design the particles and their relative interactions with exquisite precision but it is also feasible, exploiting self-assembly, to create them in bulk quantities and investigate their collective behavior. One interesting field of application is the physics of patchy colloids, particles interacting with a limited number of neighbours due to selective lock-and-key type binding. These particles have stimulated broad research for the peculiarities of their phase diagrams and unconventional physical properties.^{6–12} The performance of these patchy-systems is strongly related to the number of patches present on particles' surfaces. In the single-bond-per-patch condition, the number of patches determines the maximum number of bonds that particles are able to form and thus it is also referred to as valence *f*. For example, theoretical studies suggest that *f* controls the width of the gas-liquid phase separation.^{13,14} By reducing *f*, the phase separation boundary shifts to small densities, opening a density region in which, at low enough

temperatures (*T*), an “empty” homogeneous arrested state, or *gel*, is formed.¹³ Interestingly, it has been recently suggested that the evolutionary process has exploited the different gelation ability of proteins with small valence to construct self-assembled biologically relevant optical devices.¹⁵ Besides proteins, concepts developed for patchy colloidal particles also apply¹⁶ to telechelic and poly-functional polymers, carrying complementary end-groups, which have been investigated with the aim of controlling the strength of the resulting gel.^{17,18}

Previous experimental studies have shown the suitability of DNA to produce bulk quantities of particles in the lab to investigate the influence of *f* on the phase diagram of patchy colloids.^{4,19} Moreover, experimental studies of binary mixtures of DNA particles of valence one and valence four have been able to reproduce with high fidelity theoretical predictions¹¹ even for unconventional re-entrant gels, capitalizing on the competition between different bonding sequences.¹⁹ Here, we demonstrate how to design and implement an all-DNA system that constitutes the colloidal analog of poly-functional condensation but with the additional control of thermal reversibility and/or bond lifetime. This is a desirable step in the design of biocompatible systems with innovative dynamic properties such as DNA-*vitrimers*,²⁰ networks with self-healing properties.^{21,22} It also constitutes an advantageous stage for testing recent predictions on the long-range nature of the effective interaction between colloidal particles immersed in a solution which is itself close to percolation.²³ For this case, the ability to control the lifetime of the clusters is crucial.²⁴

We investigate, via dynamic light scattering (DLS), a binary mixture of valence four (*A*) and valence two (*B*) DNA particles, with selective *AB* bonds for different ratios

^{a)}Electronic mail: javier.fernandez.castanon@roma1.infn.it

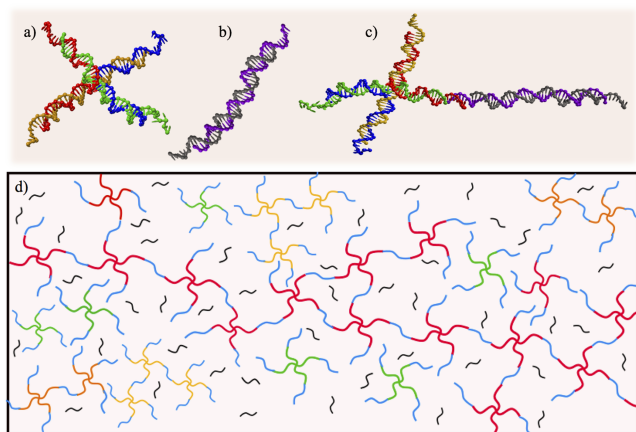


FIG. 1. Representation of the DNA-made particles, highlighting how the different single strands bind to form (a) the tetra *A* and (b) the bifunctional *B* particles. In the (c) panel, the *A* and *B* particles are shown bonded via the sticky-end sequence. (d) Schematic representation of the system beyond the percolation threshold ($r < 6.0$). The *A*-particles in the spanning percolating cluster are colored in red, clusters with one *A* particle are colored in green, clusters with two *A* particles are colored in orange, and clusters with three *A* particles are colored in golden yellow. The *B* particles linked to tetramers are plotted in blue while the non-bonded *B* particles are represented in black.

$r \equiv N_B/N_A$, where $N_A(N_B)$ indicates the number of *A*(*B*) particles [see Figs. 1(a) and 1(b)]. Specifically, we demonstrate, guided by the Flory-Stockmayer polymerization models,^{25,26} how either liquid or gel states can be produced by tuning r . Indeed, for the stoichiometric composition $r = 2$ (in which there are two *B* for each *A*), every *B* acts as a bridge between *A*s and, at low T when all possible bonds are formed, the system gels in a tetravalent structure. On increasing the concentration of *B*s, the network starts to break. At this point, some of the *B*s are connected to only one *A* particle, preventing the bridging between the tetravalent nodes of the network. For a critical r , the system reaches the percolation point where a highly polydisperse cluster size distribution is present. On further increasing the number of *B* with respect to that of *A*, the system becomes composed of isolated finite size clusters. DLS provides a clear quantification of these structural changes.

Different from covalently bonded systems we are able to control, by changing T , the *AB* bond lifetime, being thus able to observe the crossover between physical and chemical gels.

II. MATERIALS AND METHODS

A. Materials and sample preparation

Tetravalent *A* nanostars are assembled by mixing in solution equimolar quantities of four different DNA single strands (ss-DNA) (Seq. A1-A4, Fig. 2) while bivalent *B* particles by two ss-DNA (Seq. B1-B2). As shown in Fig. 1(a), the *A* nanostars are an artificial replication of the 4-way DNA intermediates or Holliday junctions^{27,28} which play a key role in homologous recombination and DNA repair and which have been of particular interest for biological studies.^{29,30} Differently from the biological relevant cases, the base sequences departing

Seq. A1.	5'-CTACTATGGCGGGTGATAAAA CGGGAAGAGCATGCCCATCCAGGACACGC-3'
Seq. A2.	5'-GGATGGGCATGCTCTTCCCGAA CTCAACTGCCTGGTGATACGAGGACACGC-3'
Seq. A3.	5'-CGTATCACCAGGCAGTTGAGAA CATGCGAGGGTCCAATACCGAGGACACGC-3'
Seq. A4.	5'-CGGTATTGGACCCCTCGCATGAA TTTATCACCCGCCATAGTAGAGGACACGC-3'
Seq. B1.	5'-GGTTGTGCTTCGCCGTTGCCG AGCGTGTCC-3'
Seq. B2.	5'-CGGCAACGGCGAAGCACAACC AGCGTGTCC-3'

FIG. 2. Sequences of DNA used in this study.

from the junction are asymmetric, preventing the sliding of the junction and thus locking the strands in the desired position. Following previous studies,^{4,31-33} the designed sequences incorporate a structural component which determines the particle formation and a binding component (the sticky-end sequence) designed to allow interparticle linking, but only between *A* and *B*. Indeed, each arm of the nanostar is composed of two complementary sequences, marked with the same color, of 20 nucleotides, while *B* particles are constituted by a double strand (ds-DNA) composed of 21-bases. Since the persistence length of ds-DNA is about 150 nucleotides, the *B* particle can be considered as a rigid rod. The two adenine nucleotides in the A1-A4 sequences labeled in red in Fig. 2 have no complementary partners in other sequences. Their role is to provide flexibility to the core of the *A* particle.⁴ The melting T (T_m) at which ss-DNA sequences pair to form ds-DNA is determined by the number of nucleotides in the bonding sequence. Since the lengths of the binding parts of the ss-DNA are comparable, both *A* and *B* particles are formed at approximately the same T (65 °C). Both *A* and *B* ends terminate with an 8-bases (emboldened in Fig. 2) long sticky sequence preceded by an extra adenine nucleotide which permits the sticky-ends to bend and to rotate, easing the linking between *A* and *B* binding sites. The smaller number of nucleotides of the sticky-ends forces the *A*-*B* bonds to start forming well below 65 °C, e.g., after the *A* and *B* structures have properly self-assembled.

Figures 1(a)-1(c) show the three-dimensional representation of the two particles and of their binding.

The presence of the adenines at the center of the sequences generates a significant flexibility of the nanostar arms. Thus we cannot exclude the possibility that both ends of a bridge particle bind with two different arms of the same nanostar. This case constitutes the simplest example of an intra-cluster bond, a possibility which is not included in the loop-free calculations of Flory and Stockmayer.³⁴ This type of intra-cluster link is expected to be more frequent at low concentration, when the probability of encountering distinct bridge particles is decreased and in the limit of small ratio of bridges to nanostars. Since we work at large concentrations (see Table I) and in the limit of large ratio of bridges to nanostars, the presence of such configuration is expected to be rare. We also note that such an intra-cluster bond transforms a nanostar into a bridge, essentially acting as a minor renormalization of the ratio r .

TABLE I. Relative ratios $r \equiv N_B/N_A$, composition $x \equiv N_A/(N_A + N_B)$, and corresponding concentrations ρ_A and ρ_B for each sample. The last three columns report mean-field theoretical predictions⁴⁰ for the case when all possible bonds are formed (low T): (i) the fraction of bonded B interacting sites p_B ; (ii) the mean number of A particles in finite size clusters (MCS); and (iii) the fraction of A particles in the infinite cluster P_∞ .

r	x	ρ_A (μM)	ρ_B (μM)	p_B	MCS	P_∞
9.0	0.10	39.76	357.86	0.22	3.7	0
6.0	0.14	56.46	341.16	0.33	77	0
4.9	0.17	67.59	330.03	0.40	5.9	0.59
2.0	0.33	132.54	265.08	1.0	0	1

DNA was provided by Integrated DNA Technologies (IDT) with PAGE purification. Equimolar concentrations of A and B ss-DNA sequences were mixed in deionized and filtered H_2O and NaCl buffers, to prepare initial volumes of solutions of A and B particles, at concentrations of $191 \mu\text{M}$ and $652 \mu\text{M}$, respectively. Nanodrop³⁵ measurements confirmed the lack of contaminants. The final NaCl concentration was fixed at 200 mM . A centrifugation process ran at $25^\circ\text{C}/4.4 \text{ krpm}$ for 10 min facilitated the complete solution of the DNA strands in the buffer. Subsequently, each sample was kept for 20 min at 90°C before being slowly cooled down back to room T overnight.

We prepared 4 samples at $r = 9.0, 4.9, 6.0,$ and 2.0 . In all samples, the concentration of the total number of particles has been fixed at the value $\approx 2.4 \times 10^{20} \text{ l}^{-1}$. Table I provides detailed information on the prepared samples.

We performed experiments in the region of concentrations where the system is homogeneous. It has been recently demonstrated that particles with small valence do phase separate in gas-like and liquid-like regions but only in a very limited range of concentrations.¹³ The phase diagram for the studied mixture has been calculated within the Wertheim formalism,^{36,37} confirming that the phase-separation region is limited to concentrations lower than the one of the fully bonded network.³⁸ To provide a feeling of the values of the selected concentrations, consider that a fully bonded ($r = 2.0$) diamond-like structure composed of tetrahedral particles linked by the bifunctional ones (as silicon and oxygen in silica, for example) would require a total molar concentration of particles (both A and B) of $\approx 400 \mu\text{M}$. Thus, all investigated samples do not suffer from phase-separation³⁸ being well inside the equilibrium-gel region.¹⁴

B. Dynamic light scattering

DLS measures the intensity correlation functions $g_2(q; t)$. Experiments were performed at a fixed angle $\theta = 90^\circ$ on a setup composed of a Newport 633 nm He-Ne laser (source power 17 mW) and a Brookhaven Instrument correlator. Volumes of $45 \mu\text{l}$ for every sample were held in borosilicate glass tubes with an internal radius of 1.5 mm and immersed in a water bath connected to a thermostat. Thermalisation intervals between 30 and 40 min were considered to optimise the proper stabilisation of the samples at every T , followed by measurements of $25\text{-}30 \text{ min}$. The electric field correlation function $g_1(q; t)$ can

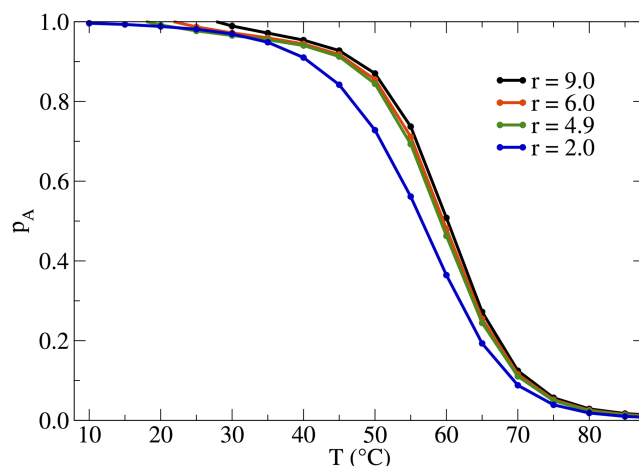


FIG. 3. Probability of observing an A binding site involved in an AB bond as a function of T , evaluated according to the SantaLucia thermodynamic formulation⁴¹ for different ratios r .

be estimated via the Siegert relation³⁹

$$g_2(q; t) = 1 + \beta |g_1(q; t)|^2, \quad (1)$$

where β represents the experimental coherence factor.

C. DNA melting curves

An additional gain of working with DNA nanoparticles is the well-characterized thermodynamic binding behavior of DNA sequences.⁴¹ This allows us to properly select the binding temperature of the sticky sequence, controlling the AB bonds. The T dependence of the bonded fraction of A and B sticky-ends p_A and p_B can be quite accurately estimated exploiting the SantaLucia thermodynamic formulation⁴¹ as coded, for example, in the open access NUPACK⁴² oligocalculator. Using as input to NUPACK the concentration of A and B sticky sequences and the 200 mM NaCl salt concentration, the program provides the T -dependence of the fraction of unbonded pairs f_{unb} which easily transforms to $p_A = (1 - f_{unb})(0.5 + r)$ and $p_B = 2p_A/r$ (see Sec. III). Figure 3 shows the predicted T -dependence of p_A for the investigated samples. p_A changes from 0 to 1 in a small T interval, centred around 60°C , with a width of about 20°C . There is a weak dependence on r originating from the progressive larger amount of B particles on increasing r . Below $T = 40^\circ\text{C}$, p_A has reached its asymptotic unit value indicating that at this T essentially all possible bonds in the system are formed.

III. THEORETICAL BACKGROUND: THE $A_4\text{-}B_2$ MIXTURES WITH ONLY AB BONDS

To grasp the motivation behind the selected values of r , we briefly review the seminal work by Flory²⁵ and Stockmayer²⁶ on the condensation of polyfunctional molecules as a function of the extent of reaction. In order to better link this theoretical formalism with our experimental research, it is desirable to introduce the *composition* x of the system as the fraction of A particles present in the system, $x \equiv N_A/(N_A + N_B)$. The values of x are listed in Table I and are related to the ratio according to $r = (1 - x)/x$. Neglecting the formation of close loops of bonds (what today we identify with the Bethe lattice⁴³) Flory and

Stockmayer were able to provide mean-field predictions for the location of the percolation (gelation) transition and for the evolution of the cluster size distribution. During the years, they focused on several chemical reaction types, including mixtures of particles of different types and functionality.³⁴ An interesting case is offered by the binary mixture of particles with functionality f ($f = 4$ in the present study) and particles with functionality two when only AB bonds are present. When this is the case, the composition of the system is defined by the number of particles of each type N_A and N_B and by the probabilities that a randomly selected A or B binding site is involved in bonds p_A and p_B . Since each bond involves one A and one B bonding site, p_A and p_B can be calculated as

$$p_A = \frac{N_{bonds}}{4N_A} \quad p_B = \frac{N_{bonds}}{2N_B}, \quad (2)$$

where N_{bonds} indicates the total number of formed bonds. Thus, the presence of only AB bonds fixes a connection between p_A and p_B through the total number of bonds

$$p_B = \frac{2p_A N_A}{N_B} = \frac{2p_A}{r}. \quad (3)$$

The fully bonded network condition (when all bonding sites are involved in bonds) requires both $p_A = 1$ and $p_B = 1$ and hence $r_{fb} = 2.0$. Another important relative composition is provided by the percolation threshold, when an infinite spanning cluster first forms. As shown in Ref. 40, this specific point is

$$p_A p_B = \frac{1}{(f-1)}. \quad (4)$$

An interesting case is the one for which the reaction has proceeded to completion, e.g., when all possible bonds are formed. This is the infinite time limit in poly-functional condensation. When $r = r_{fb}$, this corresponds to a perfect network, in which all possible binding sites are engaged into bonds. For larger values of r , all A binding sites remain bonded while some of the B sites do not participate into bonds. In all these cases ($r > r_{fb}$), $p_A = 1$ and thus $p_B = 2/r$. Similarly, when $r < r_{fb}$ all B sites are bonded, $p_B = 1$ and $p_A = r/2$. When all possible bonds are formed, percolation is thus achieved at $r = 2/3$ and $r = 6$. For intermediate values of r , an infinite spanning cluster is present, whereas for values of r outside this interval, the system is composed of polydisperse clusters of finite size.

The cluster size distribution $N(n, l)$, according to Stockmayer⁴⁰ is, indicating with n the number of particles in the cluster of type A and with l the number of particles in the cluster of type B ,

$$N(n, l) = f N_A \frac{(1-p_A)(1-p_B)}{p_B} \times \frac{(fn-n)!(2l-l)!}{(fn-n-l+1)!(2l-l-n+1)!n!l!} x_f^n x_2^l,$$

where

$$x_f = p_B \frac{(1-p_A)^{(f-1)}}{(1-p_B)},$$

$$x_2 = p_A \frac{(1-p_B)}{(1-p_A)}.$$

Note that $n-1 \leq l \leq 1+2n$. In addition, when $p_A = 1$, the value of l is slaved to the value of n by the relation

$l = 3n + 1$. From Eq. (5) it is possible to evaluate the mean cluster size MCS and the fraction of particles in the infinite cluster P_∞ (the gel). These data for the studied systems are also reported in Table I.

The mean-field predictions presented above, based on the absence of loops of bonds in finite size clusters, are bound to fail close to the percolation threshold where the cluster distribution function must deviate from the mean-field predictions to acquire the scaling behavior characteristic of the percolation universality class.⁴⁴ How close the system must be to percolation to feel the non-mean-field effects (the Ginzburg criterium⁴⁴) is a system dependent property. It has been speculated that in the case of low valence colloidal particles, the mean-field predictions are rather robust.⁴⁵ In the Appendix, we report comparisons between Eq. (5) and Monte Carlo simulations at the same r values experimentally studied to provide evidence that in this small valence systems, the mean-field predictions are sufficiently accurate (especially far from percolation) to guide the interpretation of the experimental results.

IV. RESULTS AND DISCUSSION

As previously discussed, on decreasing r , the sample changes from a collection of diffusing clusters to a percolating system and finally to a fully bonded network. The number of bonds in the system, quantified by p_A and p_B , is T dependent. Still, as shown in Fig. 3, p_A changes from 0 to 1 in a small T interval. Below 40 °C, all changes in the dynamics can be attributed to the opening and closing of the bonds and the associated reshuffling of the clusters. The lifetime of the bonds is itself T dependence and it follows an Arrhenius law with an activation enthalpy proportional to the number of bases in the sticky sequence.^{46,47}

Figure 4 shows the “fluid” case $r = 9.0$. For this r value, even when all bonds are formed, the large amount of B particles prevents the formation of large clusters. The cluster size distribution [Eq. (5)] predicts that essentially most A particles are involved in small aggregates, coexisting with several isolated B particles. The MCS (see Table I) indicates that the

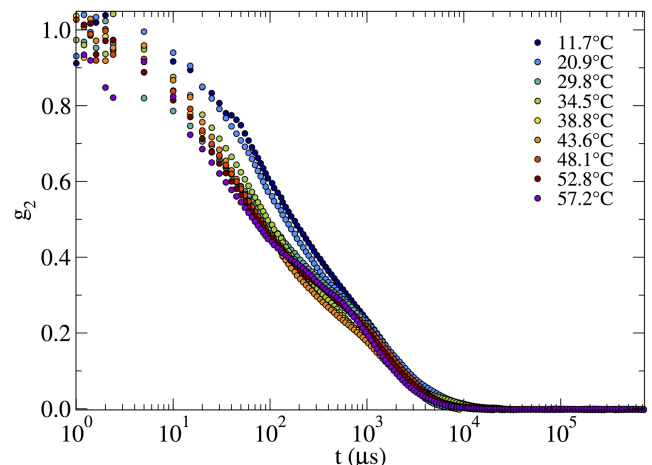


FIG. 4. DLS measurements at $r = 9.0$ where a liquid-like behavior is observed for every T .

average cluster is composed of about three A particles. Indeed, we observe that the correlation function does not significantly vary with T and it approaches zero at about $10^4 \mu\text{s}$, consistent with the expectation that the clusters in the system are of limited size and do not grow on cooling.

The sample at $r = 6.0$ corresponds to six B particles for each A particle. This r value has been selected since, according to mean-field predictions [Eq. (4)], when all possible bonds are formed, the system is close to percolation and thus composed of highly polydisperse clusters, power-law distributed in size. Different from cases in which percolation results as an effect of an irreversible polymerization process (and as such controlled by curing time), here we tune the ratio r between B and A particles to approach the percolation point. At low T , when the lifetime of the bonds is larger than the experimental time, the system is expected to behave as a chemical gel at percolation.^{45,48,49} The corresponding DLS results are presented in Fig. 5. At the highest T ($T > 53^\circ\text{C}$), the density fluctuations still decay at times comparable to those observed in the sample at $r = 9.0$ previously discussed. However, when $T < 50^\circ\text{C}$, the initial decay (which is possibly associated with the excess free B particles and to the vibrational motion within clusters) is followed by a clear logarithmic decay which extends for several decades, a signature of a highly polydisperse system.

DLS techniques have been successfully applied to investigate gelation in chemical and physical gels.^{50–54} In the limit of very dilute samples, when correlation between different clusters can be neglected, the DLS correlation function can be interpreted as resulting by the diffusive motion of the clusters (e.g., the self-component of the collective behavior). Under these conditions, the self-similarity in the cluster size, coupled to the scaling behavior of the cluster diffusion coefficient and of the size dependence of the cluster scattering intensity, generates a very wide (often power-law) decay of the density fluctuations.⁵⁰ When cluster interactions are present, the correlation function retains its very wide spectrum of decay times which can manifest as a power-law, a logarithmic behavior, or a stretched exponential decay with a small stretching exponent.⁵⁵ Our sample has a non-negligible density and

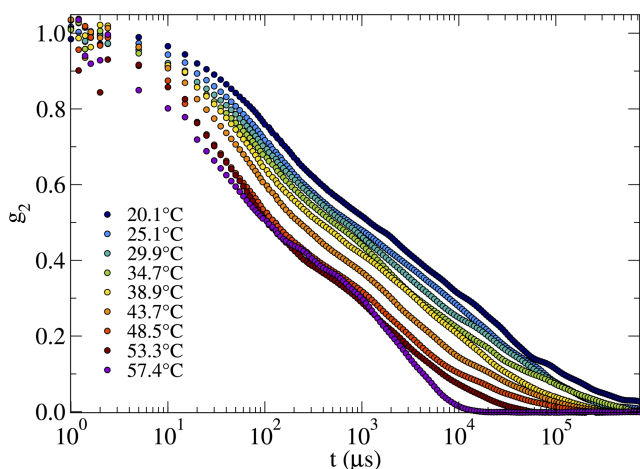


FIG. 5. DLS measurements at $r = 6.0$. Note that below 50°C all curves follow a logarithmic decay.

cluster-cluster excluded volume interactions prevent the possibility of describing the system as an ideal gas of polydisperse clusters and as such the decay of the correlation function cannot be written as a sum of independent decays. Still, the large polydispersity characterizing the proximity of the percolation point reveals itself in the observed logarithmic decay.

The third sample, prepared with $r = 4.9$, is beyond the percolation threshold. The system is composed of a spanning cluster complemented by a polydisperse set of finite size clusters, composing the sol fraction. According to Eq. (5), at low T the average number of A particles in finite size clusters is about six (see Table I), while the fraction of A particles in the infinite cluster is about 59%. The corresponding measured correlation functions are displayed in Fig. 6. Again, at $T > 50^\circ\text{C}$, most of the particles are isolated, or forming unconnected small clusters, and so the density fluctuations decorrelate at times comparable to those measured at the same T in all studied samples. The mixed nature of the sample (sol+gel) determines a complex shape of the correlation function, in which the logarithmic decay, which we attribute to the diffusion of the finite size clusters, is complemented by a more exponential decay originating from the gel component.

Finally, Fig. 7 shows the case for $r = 2.0$, matching the stoichiometry of the system with the particle valences. For this r , at low T all particles belong to the infinite cluster. The decay of the correlation function closely reproduces the one previously measured in a one-component valence-four DNA nanostar system in which the sticky-end sequence was selected to be self-complementary, enabling bonding among identical particles.⁴ In the present experiment, the bond between A particles is mediated by the presence of the B particles. Despite this difference, the decay of the correlation function is very similar, displaying a two-step relaxation process (a fast and a slow process) in which the slow decay time progressively increases on cooling. We first note that experiments in this sample are limited to $T > 36^\circ\text{C}$. For smaller T , the characteristic time becomes longer than a few seconds, which is the maximum time accessible with our light scattering apparatus. This indicates that for $T < 36^\circ\text{C}$, we can consider the system as non-restructuring for the duration of the measurement

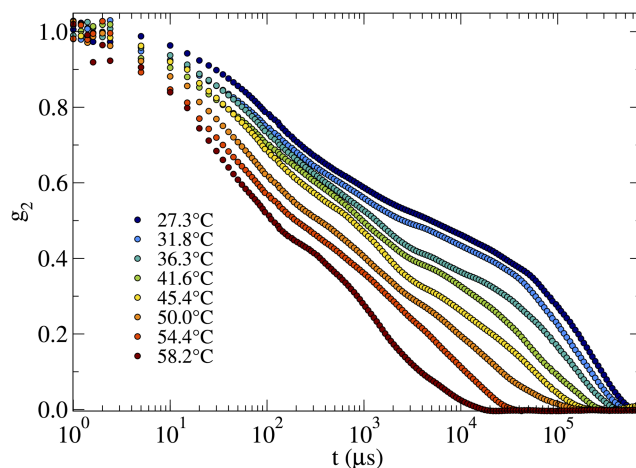


FIG. 6. DLS measurements at $r = 4.9$ where the system is beyond percolation.

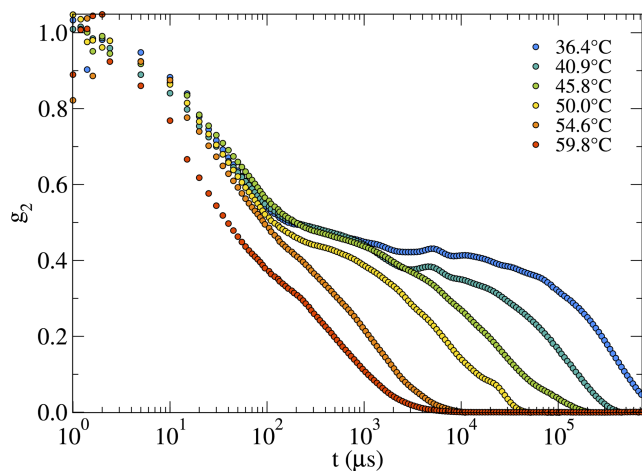


FIG. 7. DLS measurements at $r = 2.0$ where the system continuously evolves from a liquid-like behavior at high T to a gel at lower T . The relaxation time increases more than 3 orders of magnitude, while the plateau increases its height.

(chemical gel). As in Ref. 4, the correlation functions can be fitted as

$$g_1(\tau) = (1 - \alpha) \exp\left[-\left(\frac{\tau}{\tau_f}\right)\right] + \alpha \exp\left[-\left(\frac{\tau}{\tau_s}\right)^{\beta_s}\right], \quad (5)$$

where α is the amplitude of the slow process and τ_f , τ_s , and β_s stand for the fast and slow relaxation times and for the stretching exponential factor, respectively. In agreement with the valence-four nanostar case,^{4,5} β_s is comprised in the range 0.63–0.79. Also in agreement with previous data, the fast relaxation mode does not show any significant dependence on T , while τ_s follows an Arrhenius dependence (Fig. 8). The associated activation energy, $\approx 66 \pm 5$ kcal/mol, has a value comparable with the Gibbs free energy associated with the breaking/formation of the AB bonds (69 kcal/mol⁴¹). For our purposes, it is important to note that the slowing down of the dynamics reflects the progressive increase in the bond lifetime. Indeed, the bond breaking and reforming processes

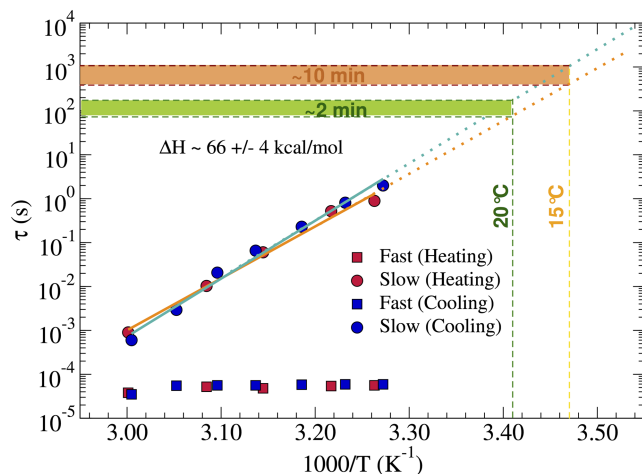


FIG. 8. Decay times τ_f and τ_s as a function of T of the x_{fb} system. Results on heating (red) and on cooling (blue) are reported. τ_s (full circles) follows an Arrhenius behavior while τ_f (full squares) does not show any detectable T dependence. Arrhenius fit to τ_s are indicated with dashed lines. The green and orange shaded surfaces indicate the 2 and 10 min time scales, corresponding to $T = 20^\circ\text{C}$ and 15°C .

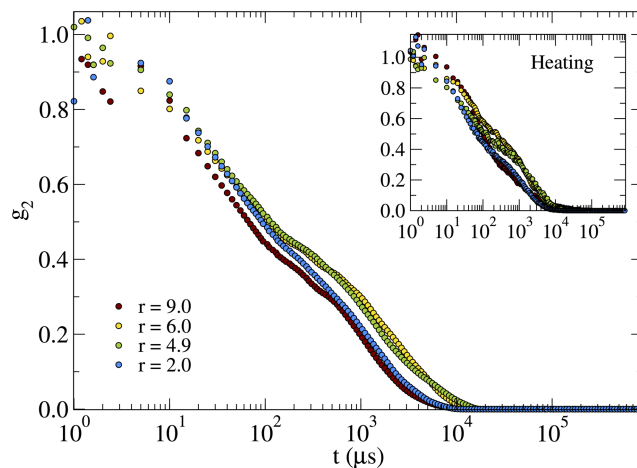


FIG. 9. DLS measurements at $T = 58^\circ\text{C}$. The decay of the correlation is rather insensitive to r . Measurements at $T = 58^\circ\text{C}$ after heating from 10°C are displayed in the inset.

constitute the elementary steps by which the local topology of the network changes, allowing the relaxation of the density fluctuations.⁵⁶

Next we compare the decay of the correlation functions at different r but at the same T , to attempt to disentangle the role of the network connectivity from the role of the bond lifetime. In Figs. 9 and 10, we show two different T values: one corresponding to a high T (58°C) where only a fraction of the possible bonds are formed (see Fig. 3) and one corresponding to 35°C . In the latter case, the structural evolution of the system is already completed and the only dynamic events altering the clusters connectivity are related to breaking and reforming of bonds. The value of τ_s measured in the $r = 2.0$ case at this two T s, an estimate of the bond lifetime, are, respectively, $10^3 \mu\text{s}$ and $10^6 \mu\text{s}$. Figure 9 demonstrates that the decay of the correlation functions at this T is very similar in all samples. This is consistent with the idea that independent of r , the clusters are small and they change their identity due to the fast bond breaking, well within the experimental sampled time window. Figure 10 shows the case of

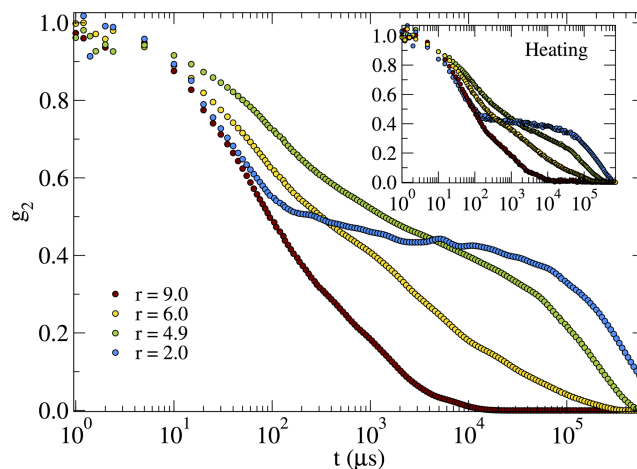


FIG. 10. DLS measurements at $T = 35^\circ\text{C}$. At this T , all possible AB bonds are formed. Measurements at 35°C after heating the samples up from 10°C are displayed in the inset.

$T = 35^\circ\text{C}$. Here extremely diversified behaviors can be observed: the crossover from a liquid (sol) to a fully bonded network state, through the percolation threshold, is spelled out. The fast decay observed for $r = 9.0$, indicating the presence of small clusters, turns into a remarkable logarithmic decay when r is close to the percolation transition, changing finally into a two-step relaxation process for smaller r , when a gel component is present.

We have repeated the experimental study on the same samples following an inverted thermalisation route, ten days after the original measurements. Starting from low T , the samples were progressively thermalised on heating, up to 57°C . The insets of Figs. 9 and 10 show a satisfactory agreement between cooling and heating ramps, demonstrating the equilibrium nature of the systems, supporting that the all-DNA design here presented is completely thermoreversible.

V. SUMMARY AND CONCLUSIONS

We have demonstrated how DNA-made particles can be designed and created in the lab to closely behave as tetra- and bi-functional units for which it is possible to control selective binding (AB binding in the present case) as well as the T at which the fully reversible binding process takes place. Specifically, we select four complementary single strands of DNA to self-assemble tetravalent A nanostars and two sequences to compose the bivalent B particles. The B particles act as bridges which connect A particles via complementary sticky overhangs attached to the particle arms. The investigated system provides the (reversible) colloidal analog of the (irreversible) A_4 - B_2 polyfunctional polymerization condensation.⁴⁴ By modulating the ratio of A and B particles, we have investigated different states on the sol-gel route, from a fluid of small clusters to a fully bonded stoichiometric gel. In addition, by selecting the binding temperature between 40 and 60°C , we have investigated both the effect of progressive bond formation and the almost chemical case, where the bond lifetime becomes longer than the accessible experimental observation time window.

Guided by the mean-field predictions of the classical models of Flory and Stockmayer⁴⁰ (and corroborated by the comparison with simulation data reported in the Appendix), we have performed light scattering experiments, probing the decay of density fluctuations. We have observed on cooling a progressive slowing down of the dynamics associated with the formation of larger and larger clusters. Below 40°C , when all possible bonds are formed, the structural evolution of the system is completed and the dynamics becomes controlled by the bond lifetime, which is represented by an Arrhenius T -dependence with an activation energy fixed by the number of base pairs of the sticky-end sequence. Around percolation, we observe a very clear logarithmic decay of the correlation function. This functional form is observed also in glass-forming systems when different competing arrest mechanisms are present.^{57–60} Logarithmic decays have also been reported in mixtures of polymeric systems⁶¹ and in glassy worm-like chain polymers.⁶² Finally, in the fully bonded case, we observe a clear two-step relaxation process. All percolating samples are examples of low valence equilibrium gel-forming systems,¹⁴ fully reversible with T .

In conclusion, we observe that the condition of full bonding is achieved in the present DNA system for $T < 40^\circ\text{C}$ (Fig. 3). According to the measure activation enthalpy, below $T < 15^\circ\text{C}$, the bond lifetime is longer than 10 min, effectively transforming the system in a stable chemical gel. Different from the chemical case, in which aggregation is irreversible and stresses are frozen in, here the process is fully reversible and a slow annealing allows the system to sample equilibrium stress-free configurations. We expect these results to be interesting for further investigations, specifically in the bottom-up self-assembling of biocompatible nanomaterials, in DNA-based plastics,²⁰ and in all cases in which a medium close to percolation is demanded.²³

ACKNOWLEDGMENTS

F.S. and J.F.-C. acknowledge support from ETN-COLLDENSE (H2020-MCSA-ITN-2014, Grant No. 642774). We thank L. Rovigatti for providing us with the schematic graphs of the A and B particles in Fig. 1 and F. Bordi for discussions and support with the experimental setup. We also thank G. Amico for technical support.

Competing financial interests: the authors declare no competing financial interests.

APPENDIX: MONTE CARLO SIMULATIONS OF A BINARY MIXTURE OF PATCHY PARTICLES

In this appendix, we report a comparison between a Monte Carlo simulation of a binary mixture of patchy particles with valence four and two and the Stockmayer theoretical predictions [Eq. (5)] with the aim of accessing the quality of the theoretical predictions and the possibility to build on the theoretical data to interpret the experimental results.

In the simulation, the particles are modeled as patchy spheres of diameter σ with patches arranged in tetrahedral (A)

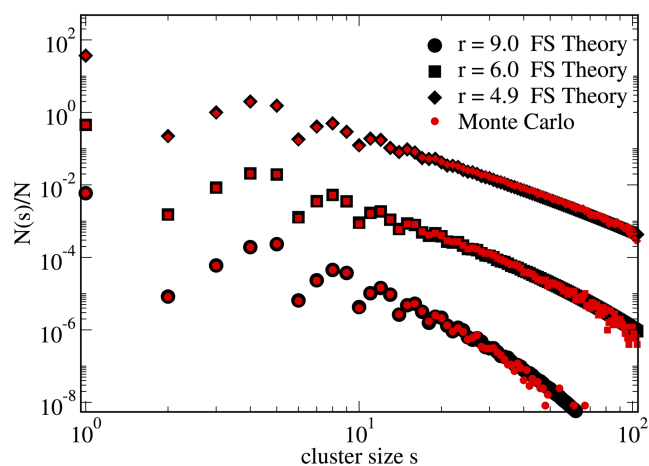


FIG. 11. Cluster size distribution $N(s)/N$ for $r = 9.0, 6.0,$ and 4.9 for $\rho\sigma^3 = 0.05$ and $k_B T/\epsilon = 0.1$ as a function of the number of particles in the cluster s . Large black symbols denote Flory-Stockmayer (FS) theoretical predictions [Eq. (5)] while smaller red symbols denote the Monte Carlo results. The curves for $r = 9.0$ have been divided by 100 while the curves for $r = 4.9$ have been multiplied by 100 to improve visibility of the comparison. The non-monotonic behavior as small cluster size s originates by the smaller probability of observing clusters with un-bonded A binding sites.

and polar (B) geometry. Particles interact via the widely used Kern-Frenkel model.⁶³ The angular square-well is defined by an opening angle $\cos \theta = 0.92$, a width of 0.15σ , and a depth of ϵ . We investigate $N = 50\,000$ particles in a cubic box of size $L = 100\sigma$ (corresponding to a number density $\rho\sigma^3 = 0.05$) with periodic boundary conditions at three of the r values studied in the experiments. Finally, to sample a reasonable number of distinct configurations, we fix $k_B T/\epsilon = 0.1$, corresponding to $p_A > 0.8$. A cluster algorithm is used to identify the clusters of bonded particles and their distribution. The number of bonds observed in equilibrium in the simulation (which coincides rather precisely with theoretical expectations calculated using the law of mass action describing a chemical equilibrium between bonded and unbonded sites; see, for example, Eqs. (4) and (5) in Ref. 45) provides via Eq. (2) the corresponding values of p_A and p_B . The resulting theoretical cluster size distributions [Eq. (5)] are compared with the corresponding Monte Carlo results in Fig. 11.

- ¹N. C. Seeman, *Annu. Rev. Biophys. Biomol. Struct.* **27**, 225 (1998).
- ²R. Bashir, *Superlattices Microstruct.* **29**, 1 (2001).
- ³A. V. Pinheiro, D. Han, W. M. Shih, and H. Yan, *Nat. Nanotechnol.* **6**, 763 (2011).
- ⁴S. Biffi, R. Cerbino, F. Bomboi, E. M. Paraboschi, R. Asselta, F. Sciortino, and T. Bellini, *Proc. Natl. Acad. Sci. U. S. A.* **110**, 15633 (2013).
- ⁵F. Bomboi, F. Romano, M. Leo, J. Fernandez-Castanon, R. Cerbino, T. Bellini, F. Bordini, P. Filetici, and F. Sciortino, *Nat. Commun.* **7**, 13191 (2016).
- ⁶J. Russo, J. Tavares, P. I. C. Teixeira, M. M. Telo da Gama, and F. Sciortino, *Phys. Rev. Lett.* **106**, 085703 (2011).
- ⁷D. de Las Heras, J. M. Tavares, and M. M. Telo da Gama, *Soft Matter* **7**, 5615 (2011).
- ⁸D. de Las Heras, J. M. Tavares, and M. M. Telo da Gama, *Soft Matter* **8**, 1785 (2012).
- ⁹Z. Zhang, A. S. Keys, T. Chen, and S. C. Glotzer, *Langmuir* **21**, 11547 (2005).
- ¹⁰F. Smallenburg and F. Sciortino, *Nat. Phys.* **9**, 554 (2013).
- ¹¹S. Roldán-Vargas, F. Smallenburg, W. Kob, and F. Sciortino, *Sci. Rep.* **3**, 2451 (2013).
- ¹²É. Duguet, C. Hubert, C. Chomette, A. Perro, and S. Ravaine, *C. R. Chim.* **19**, 173 (2016).
- ¹³E. Bianchi, J. Largo, P. Tartaglia, E. Zaccarelli, and F. Sciortino, *Phys. Rev. Lett.* **97**, 168301 (2006).
- ¹⁴F. Sciortino and E. Zaccarelli, *Curr. Opin. Colloid Interface Sci.* **30**, 90 (2017).
- ¹⁵J. Cai, J. Townsend, T. Dodson, P. Heiney, and A. Sweeney, *Science* **357**, 564 (2017).
- ¹⁶E. Bianchi, B. Capone, I. Coluzza, L. Rovigatti, and P. D. J. van Oostrum, *Phys. Chem. Chem. Phys.* **19**, 19847 (2017).
- ¹⁷T. Sakai, T. Matsunaga, Y. Yamamoto, C. Ito, R. Yoshida, S. Suzuki, N. Sasaki, M. Shibayama, and U.-i. Chung, *Macromolecules* **41**, 5379 (2008).
- ¹⁸X. Li, K. Hirose, T. Sakai, E. P. Gilbert, and M. Shibayama, *Macromolecules* **50**, 3655 (2017).
- ¹⁹F. Bomboi, S. Biffi, R. Cerbino, T. Bellini, F. Bordini, and F. Sciortino, *Eur. Phys. J. E* **38**, 64 (2015).
- ²⁰F. Romano and F. Sciortino, *Phys. Rev. Lett.* **114**, 078104 (2015).
- ²¹D. Montarnal, M. Capelot, F. Tournilhac, and L. Leibler, *Science* **334**, 965 (2011).
- ²²W. Denissen, J. M. Winne, and F. E. Du Prez, *Chem. Sci.* **7**, 30 (2016).
- ²³N. Gnan, E. Zaccarelli, and F. Sciortino, *Nat. Commun.* **5**, 3267 (2014).
- ²⁴N. Gnan, E. Zaccarelli, P. Tartaglia, and F. Sciortino, *Soft Matter* **8**, 1991 (2012).
- ²⁵P. J. Flory, *J. Am. Chem. Soc.* **63**, 3083 (1941).
- ²⁶W. H. Stockmayer, *J. Chem. Phys.* **11**, 45 (1943).
- ²⁷Y. Liu and S. C. West, *Nat. Rev. Mol. Cell Biol.* **5**, 937 (2004).
- ²⁸W. Wang, L. M. Nocka, B. Z. Wiemann, D. M. Hinckley, I. Mukerji, and F. W. Starr, *Sci. Rep.* **6**, 22863 (2016).
- ²⁹A. J. van Gool, N. M. Hajibagheri, A. Stasiak, and S. C. West, *Genes Dev.* **13**, 1861 (1999).
- ³⁰G. J. Sharples, S. M. Ingleston, and R. G. Lloyd, *J. Bacteriol.* **181**, 5543 (1999), see <http://citeseerx.ist.psu.edu/viewdoc/download?doi=10.1.1.333.7300&rep=rep1&type=pdf>.
- ³¹N. C. Seeman, *Chem. Biol.* **10**, 1151 (2003).
- ³²N. C. Seeman, *Nature* **421**, 427 (2003).
- ³³Y. Li, Y. D. Tseng, S. Y. Kwon, L. d'Espaux, J. S. Bunch, P. L. McEuen, and D. Luo, *Nat. Mater.* **3**, 38 (2004).
- ³⁴P. J. Flory, *Principles of Polymer Chemistry* (Cornell University Press, 1953).
- ³⁵P. Desjardins and D. Conklin, *J. Vis. Exp.* **45**, e2565 (2010).
- ³⁶M. Wertheim, *J. Stat. Phys.* **35**, 19 (1984).
- ³⁷M. Wertheim, *J. Stat. Phys.* **35**, 35 (1984).
- ³⁸F. Smallenburg, L. Leibler, and F. Sciortino, *Phys. Rev. Lett.* **111**, 188002 (2013).
- ³⁹B. J. Berne and R. Pecora, *Dynamic Light Scattering: With Applications to Chemistry, Biology, and Physics* (Courier Corporation, 2000).
- ⁴⁰W. H. Stockmayer, *J. Polym. Sci. A* **9**(1), 69 (1952).
- ⁴¹J. SantaLucia, *Proc. Natl. Acad. Sci. U. S. A.* **95**, 1460 (1998).
- ⁴²See <http://www.nupack.org/> for information about the analysis and design of nucleic acid systems.
- ⁴³K. Huang, *Introduction to Statistical Physics* (CRC Press, 2009).
- ⁴⁴M. Rubinstein and R. H. Colby, *Polymer Physics* (Oxford University Press, New York, 2003), Vol. 23.
- ⁴⁵J. Russo, P. Tartaglia, and F. Sciortino, *J. Chem. Phys.* **131**, 014504 (2009).
- ⁴⁶J. Šponer, J. Leszczynski, and P. Hobza, *J. Chem. Phys.* **100**, 1965 (1996).
- ⁴⁷I. Schumakovitch, W. Grange, T. Strunz, P. Bertoncini, H.-J. Güntherodt, and M. Hegner, *Biophys. J.* **82**, 517 (2002).
- ⁴⁸H. Henningá Winter *et al.*, *Faraday Discuss.* **101**, 93 (1995).
- ⁴⁹B. A. Lindquist, R. B. Jadrich, D. J. Milliron, and T. M. Truskett, *J. Chem. Phys.* **145**, 074906 (2016).
- ⁵⁰M. Adam, M. Delsanti, J. Munch, and D. Durand, *Phys. Rev. Lett.* **61**, 706 (1988).
- ⁵¹S. Richter, *Macromol. Symp.* **256**, 88 (2007).
- ⁵²S. Berthon, O. Barbieri, F. Ehrburger-Dolle, E. Geissler, P. Achard, F. Bley, A.-M. Hecht, F. Livet, G. M. Pajonk, N. Pinto *et al.*, *J. Non-Cryst. Solids* **285**, 154 (2001).
- ⁵³M. Djabourov, J.-P. Lechaire, and F. Gaill, *Biorheology* **30**, 191 (1993).
- ⁵⁴F. Bordini, G. Paradossi, C. Rinaldi, and B. Ruzicka, *Phys. A* **304**, 119 (2002).
- ⁵⁵F. Sciortino and P. Tartaglia, *Phys. A* **236**, 140 (1997).
- ⁵⁶G. Nava, M. Rossi, S. Biffi, F. Sciortino, and T. Bellini, *Phys. Rev. Lett.* **119**, 078002 (2017).
- ⁵⁷L. Fabbian, W. Götze, F. Sciortino, P. Tartaglia, and F. Thiery, *Phys. Rev. E* **59**, R1347 (1999).
- ⁵⁸F. Sciortino, P. Tartaglia, and E. Zaccarelli, *Phys. Rev. Lett.* **91**, 268301 (2003).
- ⁵⁹K. N. Pham, A. M. Puertas, J. Bergenholtz, S. U. Egelhaaf, A. Moussaid, P. N. Pusey, A. B. Schofield, M. E. Cates, M. Fuchs, and W. C. Poon, *Science* **296**, 104 (2002).
- ⁶⁰W. Götze and M. Sperl, *Phys. Rev. Lett.* **92**, 105701 (2004).
- ⁶¹A. J. Moreno and J. Colmenero, *Phys. Rev. E* **74**, 021409 (2006).
- ⁶²J. Glaser, O. Hallatschek, and K. Kroy, *Eur. Phys. J. E* **26**, 123 (2008).
- ⁶³N. Kern and D. Frenkel, *J. Chem. Phys.* **118**, 9882 (2003).